Spectroscopic studies of Ce(III) formation upon UV irradiation of aqueous pure and lanthanum-doped nanoceria

Honors Undergraduate Research Thesis

Presented in partial fulfillment of the requirements for graduation

with honors research distinction in Chemistry in the undergraduate colleges of The Ohio State University

by

Claire Alexandra Jones

The Ohio State University

April 2022

Project Advisor: Professor Bern Kohler, Department of Chemistry and Biochemistry

ABSTRACT

Cerium oxide, ‘ceria’, is a promising catalytic material with applications in catalytic converters and solid-oxide fuel cells. UV irradiation of aqueous nanoceria results in the photoreduction of Ce(IV) to Ce(III) within the lattice which is expected to be accompanied by the formation of oxygen vacancies to balance the charge of the nanoparticle. However, the adsorption of water at oxygen vacancy sites likely prevents the oxygen vacancy concentration of aqueous nanoceria from being increased through photoreduction. Doping nanoceria with rare earth ions allows its oxygen vacancy concentration to be manipulated; therefore, in the present work, lanthanum-doped polyacrylic acid-capped nanoceria was synthesized in order to investigate the effect of increased oxygen vacancy concentration on the photochemistry of aqueous nanoceria. Lanthanum incorporation was found to decrease the optical bandgap of the nanoceria. Both the lanthanum-doped and pure nanoceria samples were found to accumulate Ce(III) centers upon UV irradiation in pH 10 conditions; however, photoreduction occurred to a much greater extent in the lanthanum-doped sample possibly due to the presence of bulk oxygen vacancies which prevent recombination of bulk Ce(III) centers with photogenerated holes. Lastly, fluorescence emission spectroscopy was used in conjunction with UV-Vis absorption spectroscopy to monitor Ce(III) formation in lanthanum-doped and pure nanoceria upon UV irradiation. Photogenerated Ce(III) emission at 410 nm was found to continuously increase at similar rates in both nanoceria samples throughout the entirety of UV irradiation despite the increased photoreduction of the lanthanum-doped nanoceria sample. This suggests that photogenerated Ce(III) emission at 410 nm may exclusively be attributed to surface Ce(III) centers instead of additional photogenerated bulk Ce(III) centers that may be present in the lanthanum-doped nanoceria sample.

INTRODUCTION

Cerium(IV) oxide, or ceria, is a promising catalytic material with applications in catalytic converters and solid-oxide fuel cells (Montini et al., 2016). Ceria is able to catalyze a variety of significant chemical reactions, such as the water-gas shift reaction, carbon monoxide oxidation, and the oxidation of volatile organic compounds (Montini et al., 2016). The excellent catalytic activity of ceria can be attributed to the easy reduction of Ce(IV) to Ce(III) in the lattice, resulting in the formation of oxygen vacancies (Montini et al., 2016):

$$2Ce_{Ce} + O_o \rightarrow V_o^{\cdot\cdot} + 2Ce_{Ce}^{'} + \frac{1}{2} O_2$$

The increased oxygen vacancy concentration in ceria allows oxygen to be absorbed and released easily by the lattice, making ceria an effective catalyst for redox reactions (Sun et al., 2017).

Upon irradiation with ultraviolet light, Ce(IV) centers in aqueous ceria nanoparticles (‘nanoceria’) are photoreduced to Ce(III) centers due to the localization of photogenerated electrons on Ce(IV) ions in the nanoceria. These photogenerated Ce(III) centers then migrate to the surface of the nanoceria (Pettinger, 2019). In pH 2 conditions, Ce(III) centers at the surface of the nanoceria are released into solution as aqueous Ce(III) ions (Pettinger, 2020). However, in both basic and neutral conditions, this photodissolution of nanoceria is not favorable, and Ce(III) centers are retained at the surface of the nanoceria (Pettinger, 2019). Thus, Ce(III) formation in aqueous nanoceria under basic conditions is thought to occur until all surface sites of the nanoceria are occupied with Ce(III) before subsequently stopping (Pettinger, 2019). Although oxygen vacancies are expected to accompany the reduction of Ce(IV) to Ce(III) within nanoceria, in aqueous conditions, water has been shown to adsorb at oxygen vacancy sites on the nanoceria surface, resulting in the formation of hydroxide defects (Gritschneder and Reichling, 2007; Matolín et al., 2012). An alternative mechanism of charge compensation through the protonation of an oxide ion is therefore proposed for the photoreduction of aqueous nanoceria (Pettinger, 2019):

$$Ce_{Ce}^{'} + H^{+} + O_{o}^{x} \rightarrow Ce_{Ce}^{'} + OH_{o}^{\cdot}$$

Thus, the oxygen vacancy concentration of aqueous nanoceria likely cannot be manipulated through photoreduction. However, the incorporation of trivalent rare earth dopants such as La(III) into the ceria lattice is thought to result in the formation of oxygen vacancies to balance the negative charge introduced by the dopant (Keating et al., 2014):

$$O_{o}^{x} + 2Ce_{Ce}^{x} + La_2O_3 \rightarrow V_{o}^{\cdot\cdot} + 2La_{Ce}^{'} + 2CeO_2$$

This increase in oxygen vacancy concentration is thought to increase the catalytic activity of lanthanum-doped nanoceria relative to pure nanoceria. Zhang et al. report that the incorporation of lanthanum into ceria microspheres results in an increase in catalytic activity of the ceria towards methane combustion due to an increase in oxygen storage capacity (2010). In addition, Chahal et al. report that increasing lanthanum content in lanthanum-doped nanoceria results in an increase in photocatalytic activity towards the degradation of Rose Bengal dye (2020) This increase in photocatalytic activity was attributed to an increase in oxygen vacancy concentration as well as a decrease in the optical bandgap of the nanoceria with increasing lanthanum content, increasing the rate of excitation of electrons to the conduction band upon UV irradiation (Chahal et al., 2020) Thus, the incorporation of lanthanum as a dopant into the ceria lattice allows the oxygen vacancy concentration of the nanoceria to be manipulated, resulting in significant effects on the photochemistry of the nanoceria that have important implications in photocatalysis.

The photoreduction of aqueous nanoceria upon UV irradiation can be monitored using ultraviolet-visible (UV-Vis) absorption spectroscopy. Figure 1 shows the band diagram of ceria, consisting of an O 2p valence band, a narrow Ce 4f band, and a higher energy Ce 5d band.

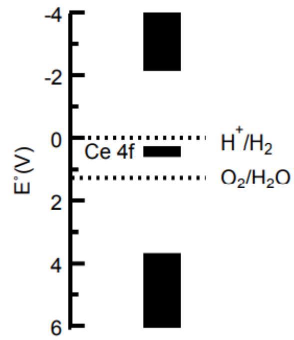

Figure 1. Electronic band structure of cerium oxide taken from Pettinger (2019) with band potentials from Dorenbos (2014).

Nanoceria absorbs strongly with an absorption onset at approximately 400 nm and an absorption maximum at approximately 290 nm due to electronic transitions between the O 2p valence band and the Ce 4f band (Marabelli et al., 1987; Pettinger, 2019). As Ce(IV) centers are reduced to Ce(III), there is a noticeable decrease in Ce(IV) absorption in the UV-Vis absorption spectrum. Damatov et al. report that the decrease in Ce(IV) absorption at 340 nm is linearly correlated with the formation of Ce(III) centers in oleate-capped nanoceria and methoxyacetic acid-capped nanoceria upon irradiation with UV light (2018). This decrease in Ce(IV) absorption is also accompanied by a blueshift in the absorption onset of the nanoceria corresponding to the filling of the Ce 4f band with photogenerated electrons (Pettinger, 2019). As the Ce 4f band fills with electrons, lower-energy transitions are no longer available to electrons in the O 2p valence band, resulting in an apparent blueshift in Ce(IV) absorption (Pettinger, 2019). Thus, changes in the magnitude of Ce(IV) absorption as well as the position of the Ce(IV) absorption onset can indicate Ce(III) formation in aqueous nanoceria upon irradiation with UV light. Previous work by Pettinger has shown that after irradiation of aqueous polyacrylic acid-capped nanoceria at pH 10 conditions, there is an increase in fluorescence emission at 405 nm that can be attributed to the formation of Ce(III) centers within the nanoceria (2019). In addition, Klochkov et al. report an increase in emission at approximately 425 nm after 30 minutes of UV irradiation of citrate-capped nanoceria (2018). This begs the question of whether fluorescence emission spectroscopy can be used in conjunction with UV-Vis absorption spectroscopy to monitor changes in Ce(IV) oxidation state during UV irradiation.

In the present work, polyacrylic acid-capped lanthanum-doped nanoceria ([La] = 25 mol %) was first synthesized to observe the effect of increased oxygen vacancy concentration on the photochemistry of aqueous nanoceria. The pure and lanthanum-doped polyacrylic acid-capped nanoceria samples were first characterized by UV-Vis absorption spectroscopy and Raman spectroscopy to gain insight into their electronic structures and oxygen vacancy concentrations. The effect of increased oxygen vacancy concentration on photogenerated Ce(III) formation within aqueous nanoceria was then investigated through monitoring changes in the UV-Vis absorption spectra and fluorescence emission spectra of the pure and lanthanum-doped polyacrylic acid-capped nanoceria samples upon irradiation with UV light.

EXPERIMENTAL

Materials

Cerium(III) nitrate hexahydrate ($Ce(NO_3)_3 \cdot 6H_2O$, Acros Organics, 99.5%), lanthanum(III) nitrate hexahydrate ($La(NO_3)_3 \cdot 6H_2O$, Sigma Aldrich, 99.999%), poly(acrylic acid) (PAA; Sigma Aldrich), and ammonium hydroxide (28-30% in water, Fisher Chemical) were used as received from the manufacturers.

Synthesis of PAA-CeO_2 and 25 mol % PAA-La-CeO_2

Polyacrylic acid-capped lanthanum-doped nanoceria (PAA-La-CeO_2; [La(III)] = 25 mol %) was synthesized via a modification of the synthesis performed by Asati et al (2009). $La(NO_3)_3{\cdot}6H_2O$ (108 mg, 0.250 mmol) and $Ce(NO_3)_3{\cdot}6H_2O$ (322 mg, 0.742 mmol) were first dissolved in 5 mL of nanopure water under stirring. The $La(NO_3)_3$ – $Ce(NO_3)_3$ aqueous solution was then added to 30 mL of ammonium hydroxide under stirring, causing the reaction mixture to change from colorless to light yellow. After approximately 1 min, 5.0 mL of a 1 g/mL polyacrylic acid solution was added to the reaction mixture under stirring in 1 mL portions. The mixture was then allowed to react in air at room temperature under stirring for 3 hours. During this time, the reaction mixture turned from light yellow to dark purple-brown in color. After 3 hours, the reaction mixture was centrifuged at 4000 rpm for 30 minutes to remove any agglomerates present. The supernatant was then isolated for a second centrifugation at 4000 rpm for 30 minutes. The resulting supernatant containing the suspended polyacrylic acid-capped nanoceria was then kept for further study. A control sample of pure polyacrylic acid-capped nanoceria (PAA-CeO_2) was synthesized via the same procedure; however, this synthesis used a metal precursor solution that only contained $Ce(NO_3)_3{\cdot}6H_2O$ (435 mg, 1.00 mmol).

UV-Vis spectroscopic measurements

UV-Vis absorption spectroscopic measurements were performed on the aqueous PAA-CeO_2 and PAA-La-CeO_2 samples using an Agilent Cary 5000 UV-Vis-NIR spectrophotometer. All measurements were performed in double beam mode with a solvent correction for water using a 1 cm fused silica cuvette.

Raman spectroscopic measurements

Solution-phase Raman spectroscopic measurements were performed on the PAA-CeO_2 and PAA-La-CeO_2 samples with a Renishaw Raman IR microprobe using a laser wavelength of 514 nm.

Fluorescence spectroscopic measurements

Fluorescence emission and excitation spectroscopic measurements were performed on the aqueous PAA-CeO_2 and PAA-La-CeO_2 samples using a Horiba QuantaMaster-8075-22 fluorimeter. All measurements were performed on samples using a 1 cm path length in a fused silica cuvette.

Aging of PAA-CeO_2 and PAA-La-CeO_2 samples

To investigate the change in UV-Vis absorption of the PAA-CeO_2 and PAA-La-CeO_2 samples over time, UV-Vis absorption spectra were taken of aqueous solutions containing 350 μL of PAA-CeO_2 or PAA-La-CeO_2 stock solution in 3.150 mL of nanopure water 1, 2, 26, and 39 days after synthesis.

Photoreduction of PAA-CeO_2 and PAA-La-CeO_2 samples 26 and 39 days after synthesis

During photoreduction experiments, 350 μL of either PAA-CeO_2 or PAA-La-CeO_2 stock solution was added to 3.150 mL of nanopure water in a 1 cm fused silica cuvette. The pH of the samples studied ranged from 10.19 to 10.46. The resulting solutions were then irradiated under stirring in a carousel photoreactor with UV light from Hg lamps. UV-Vis absorption spectra of the PAA-CeO_2 or PAA-La-CeO_2 samples were taken every 10 minutes during UV irradiation to monitor Ce(III) formation in the nanoparticles.

Monitoring photogenerated Ce(III) formation using fluorescence spectroscopy

During photoreduction experiments using fluorescence spectroscopy, either 23 μL of PAA-CeO_2 stock solution or 27 μL of PAA-La-CeO_2 stock solution were added to a 1 cm fused silica cuvette. Nanopure water was then added to the cuvette to bring the volume to 3.0 mL. The pH of the PAA-CeO_2 solution was 10.11, while the pH of the PAA-La-CeO_2 solution was 10.10. The PAA-CeO_2 and PAA-La-CeO_2 samples were then irradiated under stirring for 60 minutes in a carousel photoreactor with UV light from Hg lamps. After each irradiation interval, UV-Vis absorption spectra, fluorescence emission spectra, and fluorescence excitation spectra were taken of the samples in that order.

RESULTS AND DISCUSSION

Synthesis of PAA-CeO_2 and PAA-La-CeO_2

Photos from the synthesis of the PAA-CeO_2 and PAA-La-CeO_2 samples are shown in Figure 2. The precursor solution of $La(NO_3)_3$ and $Ce(NO_3)_3$ (or just $Ce(NO_3)_3$ in the case of the pure PAA-CeO_2 sample) salts was clear and colorless; however, adding the precursor solution to aqueous ammonium hydroxide caused the reaction mixture to immediately turn light yellow (Photo 2a). After the addition of the polyacrylic acid capping ligand, the reaction mixture turned a purple-brown color over the next three hours which gradually changed to darker brown due to the formation of ceria nanoparticles (Photo 2b). This agrees well with literature descriptions of nanoceria synthesis from the hydrolysis of Ce(III) salts. Chen and Chang report that upon the addition of ammonia to a solution of cerium(III) nitrate in various water/alcohol solvents, an initial yellow precipitate is formed which is followed by a color change to purple during synthesis (2004). This initial yellow precipitate is thought to be cerium(III) hydroxide (Chen and Chang, 2004). After the precipitation of cerium(III) hydroxide, Ce(III) is oxidized to Ce(IV) due to the alkaline conditions of the synthesis, resulting in the formation of cerium(IV) hydroxide (Chen and Chang, 2004). Dehydration is then thought to occur, resulting in the formation of nanoceria (Chen and Chang, 2004). Prior to centrifugation, the PAA-CeO_2 and PAA-La-CeO_2 reaction mixtures were brown in color (Photo 2c). Immediately after synthesis, the PAA-CeO_2 and PAA-La-CeO_2 suspensions were brownish-yellow in color (Photo 2d). Upon aging overnight, the color of the PAA-CeO_2 and PAA-La-CeO_2 suspensions changed to light yellow, indicating that Ce(IV) was still forming in the nanoceria samples during this time (Photo 2e). Two days after synthesis, the final light-yellow color of the PAA-La-CeO_2 suspension was found to be less intense than the color of the PAA-CeO_2 sample (Photo 2f). This is likely due to the lower concentration of Ce(III) precursor used during the synthesis of the PAA-La-CeO_2 sample, resulting in a lower final concentration of Ce(IV).

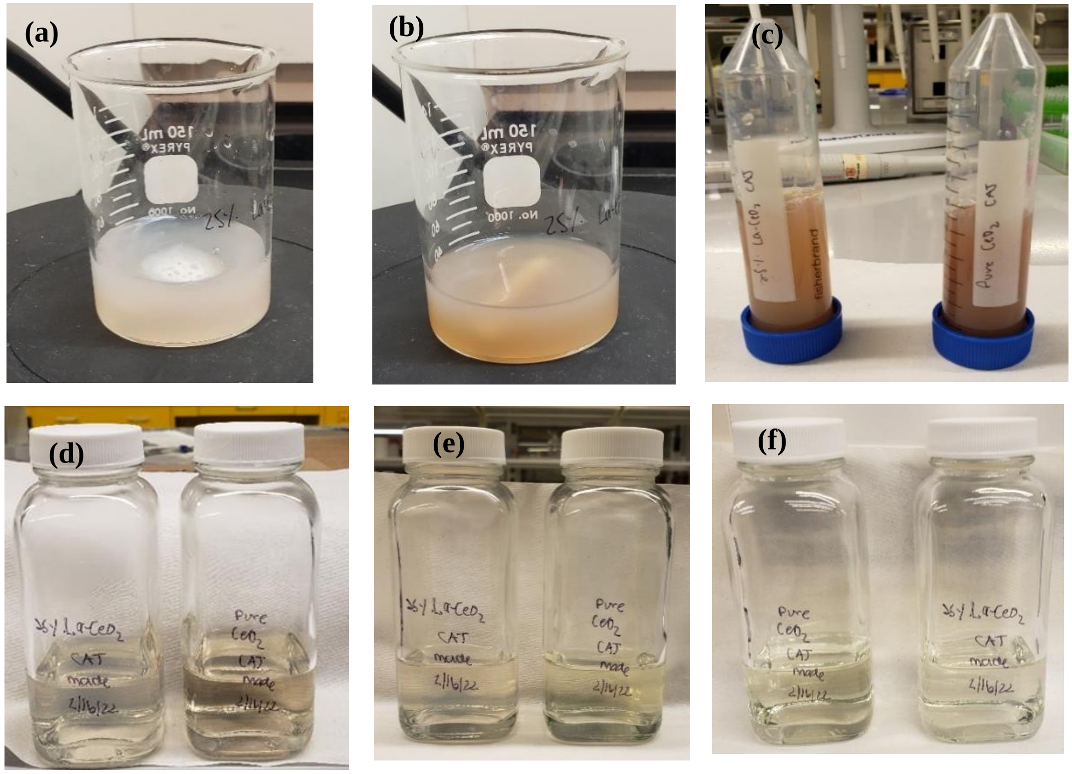

Figure 2. (a) PAA-La-CeO_2 sample immediately after mixing with NH_4OH and after the addition of PAA. (b) PAA-La-CeO_2 sample 3 hours after the addition of PAA. (c) PAA-La-CeO_2 (left) and PAA-CeO_2 (right) samples prior to centrifugation. (d) PAA-La-CeO_2 (left) and PAA-CeO_2 (right) samples immediately after synthesis. (e) PAA-La-CeO_2 (left) and PAA-CeO_2 (right) samples one day after synthesis. (f) PAA-CeO_2 (left) and PAA-La-CeO_2 (right) samples two days after synthesis.

Characterization via UV-Vis Absorption Spectroscopy

Figure 3 shows UV-Vis absorption spectra normalized at 295 nm of the PAA-CeO_2 and PAA-La-CeO_2 samples taken 48 hours after synthesis. The shapes of the UV-Vis absorption spectra of the samples differ significantly. The PAA-La-CeO_2 sample possesses an absorption onset that is redshifted compared to the absorption onset of the PAA-CeO_2 sample. This is consistent with a decrease in the optical bandgap of nanoceria upon the incorporation of lanthanum as reported by Chahal et al. (2020).

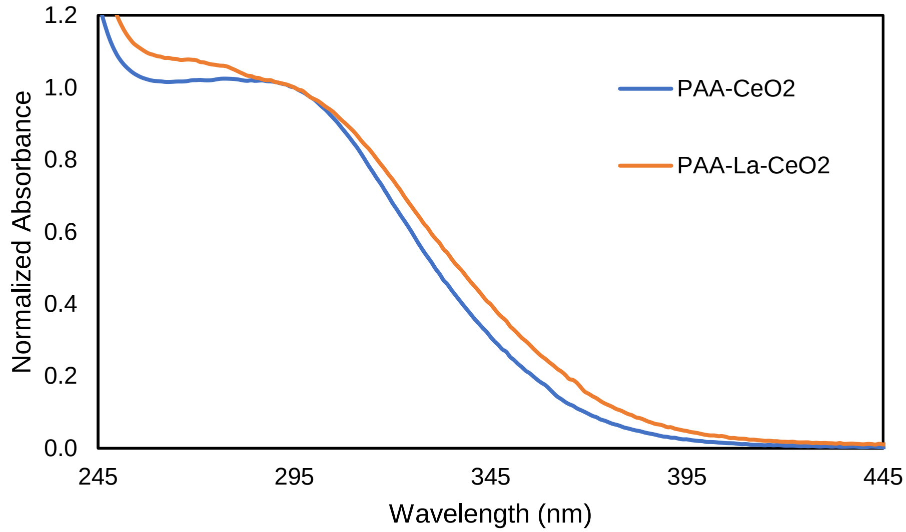

Figure 3. UV-Vis absorption spectra of the PAA-CeO_2 and PAA-La-CeO_2 samples taken 2 days after synthesis. The spectra have been normalized at 295 nm for ease of comparison.

Characterization via Raman Spectroscopy

To investigate the oxygen vacancy concentrations of the PAA-CeO_2 and PAA-La-CeO_2 samples, the samples were characterized using solution-phase Raman spectroscopy. Raman spectra of the PAA-CeO_2 and PAA-La-CeO_2 samples are shown in Figure 4. Both samples have a Raman peak at approximately 465 cm^{-1} that can be attributed to the F_{2g} mode of the ceria fluorite lattice, indicating that the crystal structures of the two samples are the same (McBride et al., 1994). When rare earth ions are incorporated into nanoceria as dopants, the F_{2g} Raman peak has been found to broaden and become less symmetric (McBride et al., 1994). The F_{2g} Raman peak of the PAA-La-CeO_2 sample is slightly broader than the F_{2g} peak of the PAA-CeO_2 sample; however, the noise in the Raman spectra of the samples prevents this from being confidently concluded. When lanthanum is incorporated into the nanoceria lattice, charge compensation is expected to occur through the generation of oxygen vacancies (Keating et al., 2014). Oxygen vacancies formed in nanoceria upon the inclusion of rare earth dopants into the lattice are known to result in a Raman peak at approximately 570 cm^{-1} (McBride et al., 1994). In the PAA-La-CeO_2 sample, there is increased intensity in the Raman spectrum at approximately 580 cm^{-1} that is absent in the Raman spectrum of the pure PAA-CeO_2 sample. However, this increased intensity at 580 cm^{-1} cannot be conclusively assigned as a peak in the Raman spectrum due to the poor signal-to-noise ratio of the Raman spectra of both nanoceria samples. Thus, characterization via Raman spectroscopy can neither confirm nor rule out the presence of increased oxygen vacancies in the PAA-La-CeO_2 sample compared to the PAA-CeO_2 sample.

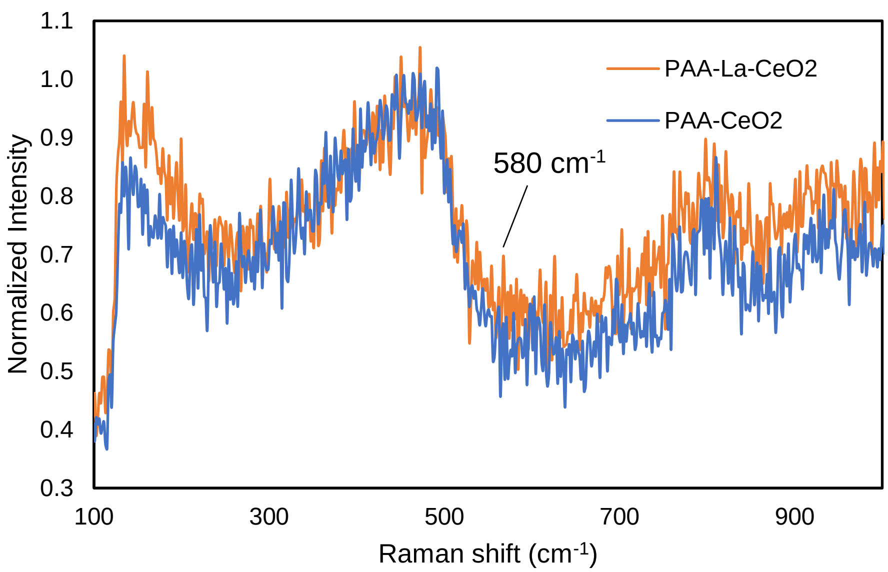

Figure 4. Raman spectra of the PAA-CeO_2 and PAA-La-CeO_2 samples taken using a laser excitation wavelength of 514 nm.

Aging of the PAA-CeO_2 and PAA-La-CeO_2 Samples

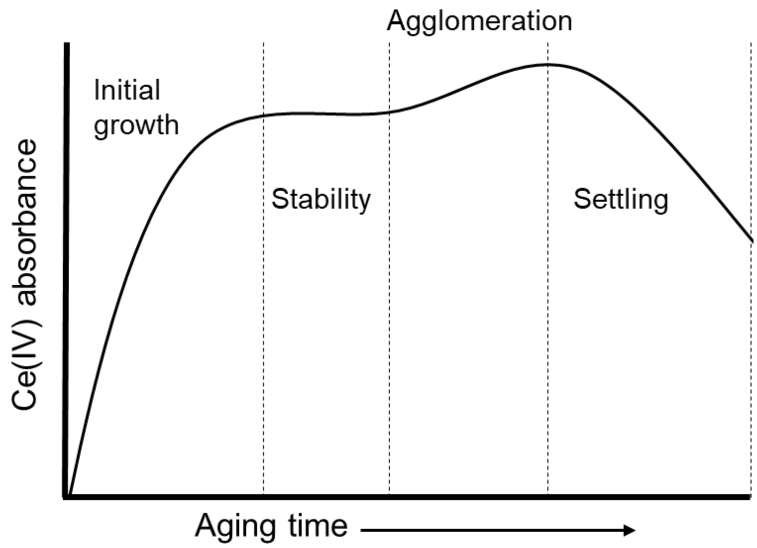

Figure 5. Expected changes in Ce(IV) absorbance at 290 nm as the PAA-CeO_2 and PAA-La-CeO_2 samples age after synthesis.

Figure 5 shows how the Ce(IV) absorbance of the PAA-CeO_2 and PAA-La-CeO_2 samples are expected to change over time as they age. Initially after synthesis, there is expected to be a rapid increase in Ce(IV) absorbance due to oxidation of the Ce(III) precursor to Ce(IV) and formation of the nanoceria. This occurs until the nanoceria has completely formed in both samples and is followed by a period of stability. Over time, the suspended nanoceria slowly agglomerates, resulting in an increase in Ce(IV) absorbance that is due to increased scattering from the larger agglomerated nanoparticles. This should also be accompanied by an increase in turbidity of the nanoceria solution. After the nanoceria agglomerates, the agglomerated nanoparticles are expected to settle out of solution, resulting in a decrease in Ce(IV) absorbance.

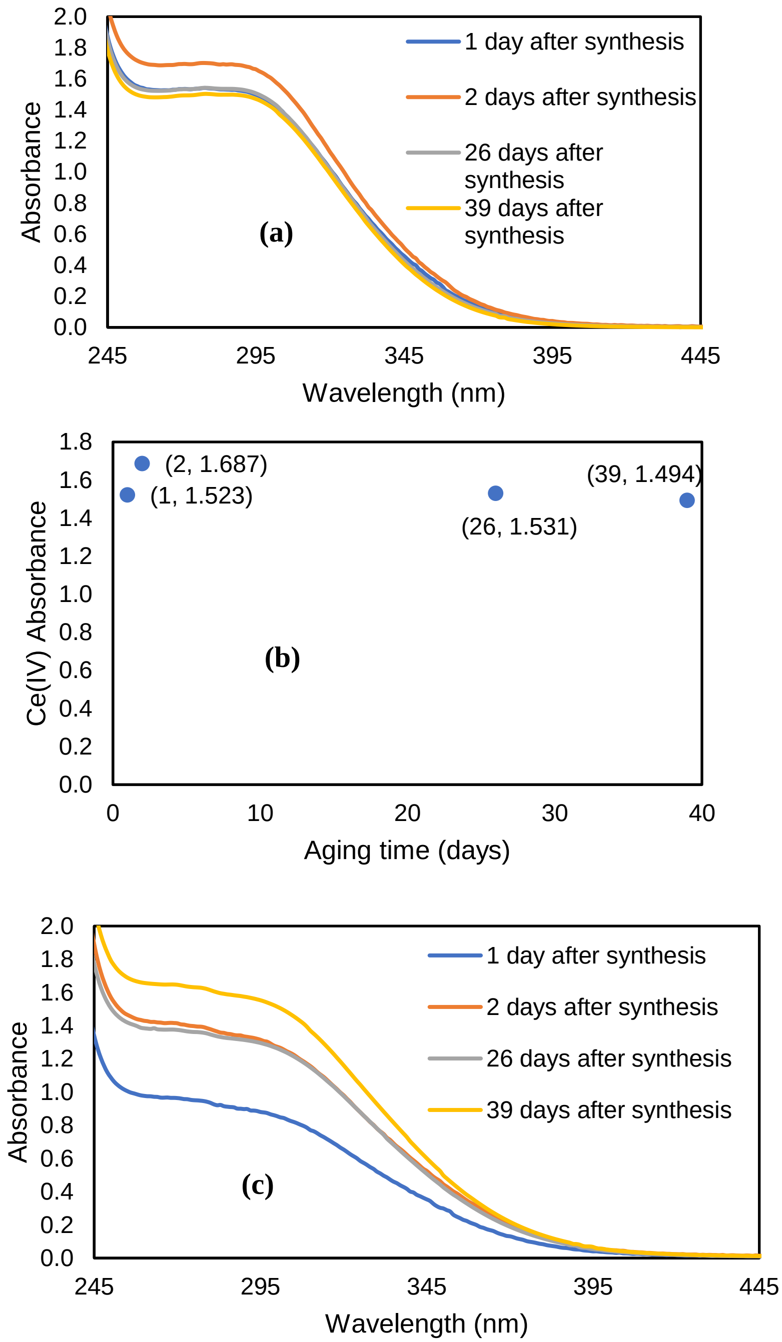

Absorbance
Wavelength (nm)
1 day after synthesis
2 days after synthesis
26 days after synthesis
39 days after synthesis
(a)
(2, 1.687)
(1, 1.523)
(26, 1.531)
(39, 1.494)
Ce(IV) Absorbance
Aging time (days)
(b)
(c)

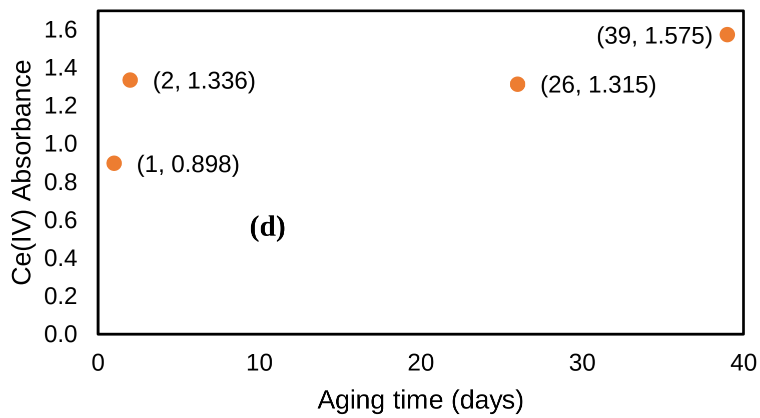

Figure 6. (a) UV-Vis absorption spectra of the PAA-CeO_2 sample taken 1, 2, 26, and 39 days after synthesis. (b) Ce(IV) absorbance at 290 nm as a function of aging time in the PAA-CeO_2 sample. (c) UV-Vis absorption spectra of the PAA-La-CeO_2 sample taken 1, 2, 26, and 39 days after synthesis. (d) Ce(IV) absorbance at 290 nm as a function of aging time in the PAA-La-CeO_2 sample.

UV-Vis absorption spectra of the PAA-CeO_2 sample taken 1, 2, 26, and 39 days after synthesis are shown in Figure 6a, while changes in Ce(IV) absorbance at 290 nm as a function of aging time for the PAA-CeO_2 sample are shown in Figure 6b. The corresponding UV-Vis absorption spectra of the PAA-La-CeO_2 sample taken 1, 2, 26, and 39 days after synthesis are shown in Figure 6c, while changes in Ce(IV) absorbance at 290 nm over time for the PAA-La-CeO_2 sample are displayed in Figure 6d. From one to two days after synthesis, there are significant increases in Ce(IV) absorbance at 290 nm of 0.164 (11%) and 0.438 (49%) for the PAA-CeO_2 and PAA-La-CeO_2 samples, respectively. This indicates that Ce(IV) centers are still forming in the nanoceria samples during this time. Aqueous Ce(III) is not stable in the alkaline conditions of the synthesis (Bouchaud et al., 2012); thus, this increase in Ce(IV) absorbance at 290 nm from 1 to 2 days after synthesis is likely due to the oxidation of Ce(III) centers initially formed in the nanoceria lattice upon synthesis to Ce(IV) instead of the formation of new nanoceria from leftover Ce(III) precursor. The much larger increase in Ce(IV) absorption seen for the PAA-La-CeO_2 sample compared to the PAA-CeO_2 sample suggests the oxidation of Ce(III) centers within the PAA-La-CeO_2 sample occurs on a longer timescale compared to the oxidation of Ce(III) centers formed within the PAA-CeO_2 sample. This suggests that bulk Ce(III) centers may be more stable in the PAA-La-CeO_2 sample upon synthesis compared to the PAA-CeO_2 sample. This can be explained by an increase bulk oxygen vacancy concentration present in the PAA-La-CeO_2 sample upon incorporation of the lanthanum dopant. Oxygen vacancies have been shown to stabilize polarons such as Ce(III) centers in nanoceria (Sun et al., 2017). Thus, an increased bulk oxygen vacancy concentration of the PAA-La-CeO_2 sample could be responsible for the slower oxidation of Ce(III) centers in the lattice to Ce(IV) centers upon synthesis.

From 2 to 39 days after synthesis, there is a decrease in Ce(IV) absorbance at 290 nm of 11% in the PAA-CeO_2 sample that is consistent with the nanoparticles gradually beginning to settle out of solution at long times after synthesis; however, a noticeable precipitate was not observed in the PAA-CeO_2 sample 39 days after synthesis. This settling period would have been preceded by a period of agglomeration that could have occurred in between 2 and 26 days after synthesis. Thus, due to the lack of UV-Vis absorption spectra taken at additional timepoints between 2, 26, and 39 days after synthesis, it is difficult to determine the time period in which the PAA-CeO_2 sample was stable in solution after synthesis.

From 2 to 26 days after synthesis, the Ce(IV) absorbance in the PAA-La-CeO_2 sample was found to decrease by just 1.5%, indicating that the PAA-La-CeO_2 is likely stable in solution from 2 to 26 days after synthesis. From 26 to 39 days after synthesis, the Ce(IV) absorbance at 290 nm increased by 20% in the PAA-La-CeO_2 sample, indicating that the nanoparticles had begun to agglomerate. This was further supported by the increased turbidity of the PAA-La-CeO_2 stock solution at 39 days after synthesis.

The PAA-La-CeO_2 sample was synthesized using a target lanthanum content of 25%; thus, it is expected that the final Ce(IV) absorbance of the PAA-La-CeO_2 sample at 290 nm would be 75% of the final Ce(IV) absorbance of the PAA-CeO_2 sample at 290 nm. Two days after synthesis, the Ce(IV) absorbance of the PAA-La-CeO_2 sample measured at 290 nm was found to be 79% of the Ce(IV) absorbance of the PAA-CeO_2 sample measured at 290 nm. Given that all starting La(III) was incorporated into the nanoceria as a dopant, this suggests that the PAA-La-CeO_2 sample possesses a lanthanum content of 21 mol %. However, the lack of UV-Vis absorption spectra at timepoints in between 2 days and 26 days after synthesis makes it difficult to accurately determine the final equilibrium Ce(IV) absorbance of the PAA-CeO_2 and PAA-La-CeO_2 samples. Further characterization via elemental techniques such as X-ray fluorescence spectroscopy is needed to provide greater insight into the lanthanum content of the PAA-La-CeO_2 sample.

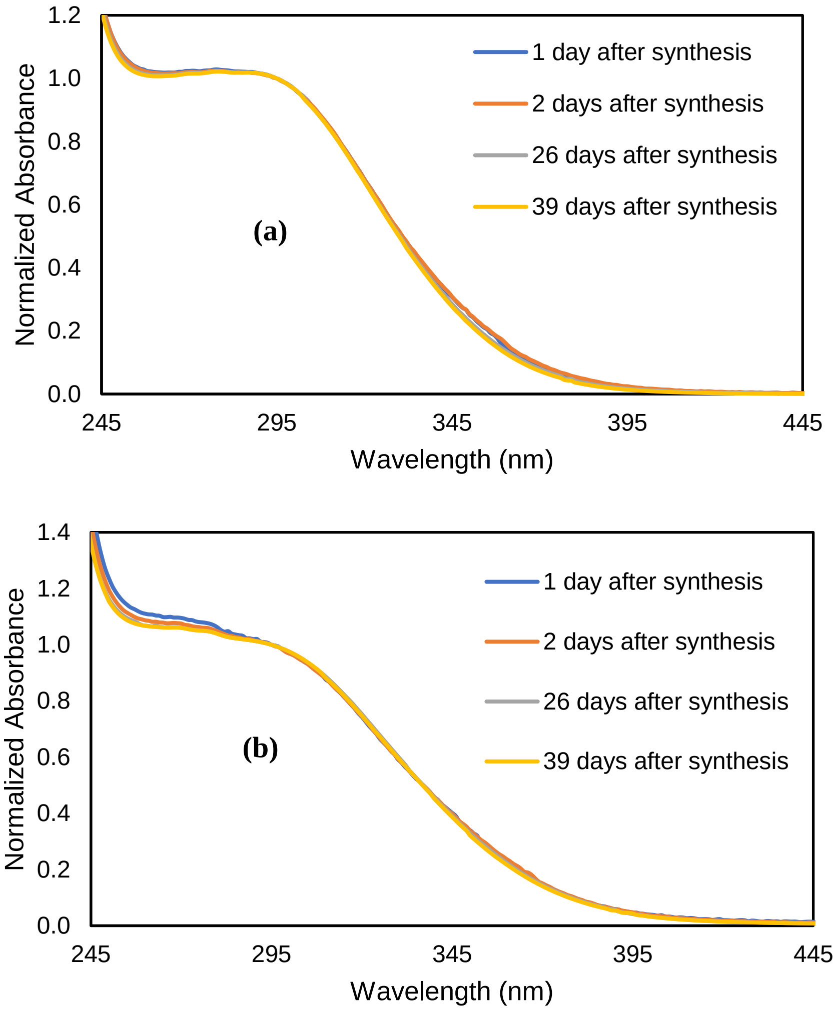

Figure 7. UV-Vis absorption spectra of the (a) PAA-CeO_2 and (b) PAA-La-CeO_2 samples taken 1, 2, 26, and 39 days after synthesis. The spectra have been normalized at 295 nm.

Figure 7 shows UV-Vis absorption spectra of the PAA-CeO_2 and PAA-La-CeO_2 samples taken 1, 2, 26 and 39 days after synthesis normalized at 295 nm for ease of comparison. For both samples, there is a decrease in shorter wavelength absorption from approximately 250 nm to 280 nm which appears to be more pronounced in the PAA-La-CeO_2 sample. However, the changes in the shape of the UV-Vis absorption spectra of both samples are very slight. This indicates that no novel chemical species are being formed in the sample stock solutions over time. In addition, this indicates that the redshifted absorption onset of the PAA-La-CeO_2 sample is retained as the sample ages.

Photoreduction of the PAA-La-CeO_2 and PAA-CeO_2 samples 26 and 39 days after synthesis

UV irradiation experiments were performed on fresh PAA-CeO_2 and PAA-La-CeO_2 samples 26 and 39 days after synthesis to investigate whether the expected increase in oxygen vacancy concentration upon the incorporation of lanthanum affects the photoreduction of aqueous nanoceria. Figure 8 shows UV-Vis absorption spectra of the PAA-CeO_2 sample taken every 10 minutes during UV irradiation 26 days after synthesis. From 0 to 40 minutes of UV irradiation, there is a 12% decrease in Ce(IV) absorption at 290 nm accompanied by a blueshift in the absorption onset of the PAA-CeO_2 sample. This suggests that during the first 40 minutes of UV irradiation, Ce(IV) centers in the PAA-CeO_2 sample are being photoreduced to Ce(III) centers. From 40 to 60 minutes of irradiation, there is a slight 0.95% increase in Ce(IV) absorption at 290 nm which is not accompanied by a noticeable shift in the absorption onset. This suggests that photoreduction of Ce(IV) to Ce(III) in the PAA-CeO_2 sample has stopped after 40 minutes of irradiation. There are two possible explanations for the slight increase in Ce(IV) absorbance at 290 nm from 40 to 60 minutes of UV irradiation. First, photogenerated Ce(III) centers may have begun to slowly be oxidized to Ce(IV) by oxygen in solution during this time. Klochkov et al. report that Ce(IV) absorbance of photoreduced citrate-capped nanoceria at pH 6.5-7.0 fully recovers one day after UV irradiation (2018). The oxidation of photogenerated Ce(III) to Ce(IV) is not induced by UV irradiation and has been found to occur at a much longer timescale than photoreduction (Klochkov, 2018). Thus, due to the short time between the end of photoreduction in the PAA-CeO_2 sample and the increase in Ce(IV) absorbance at 290 nm, a more probable explanation is that the photoreduced nanoparticles have begun to agglomerate upon further UV irradiation. Upon photoreduction of the nanoceria, photogenerated holes are thought to be scavenged by polyacrylic acid capping ligands, which causes them to degrade (Pettinger, 2019). The degradation of polyacrylic acid causes the nanoceria to be unstable in solution and begin to agglomerate, resulting in an increase in Ce(IV) absorbance due to increased scattering from the agglomerated nanoparticles (Pettinger, 2019).

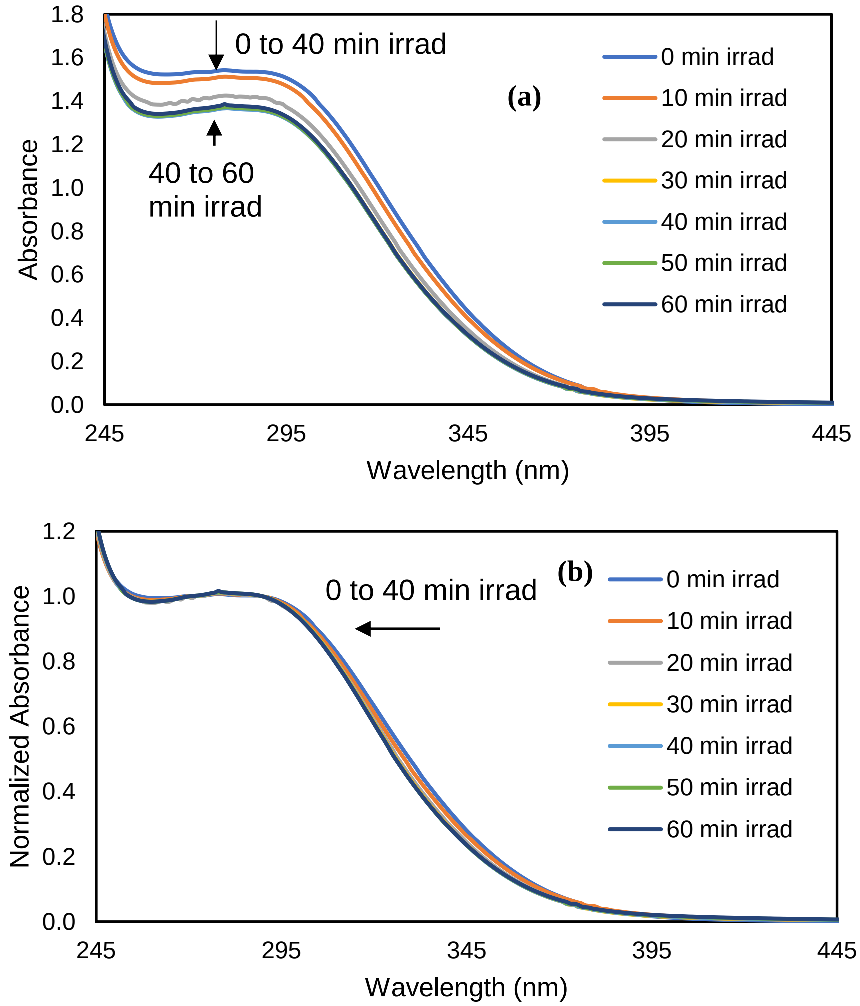

Figure 8. UV-Vis absorption spectra of the PAA-CeO_2 sample taken every 10 minutes during UV irradiation 26 days after synthesis. (b) All UV-Vis absorption spectra in (a) normalized at 290 nm.

UV-Vis absorption spectra of the PAA-CeO_2 sample taken every 10 minutes during UV irradiation 39 days after synthesis are displayed in Figure 9. During the first 40 minutes of UV irradiation, there is a 7.0% decrease in Ce(IV) absorption at 290 nm which is accompanied by a blueshift in the absorption onset of the PAA-CeO_2 sample. These results indicate that, similar to the PAA-CeO_2 sample irradiated 26 days after synthesis, Ce(IV) centers are being reduced to Ce(III) in the PAA-CeO_2 sample during the first 40 minutes of irradiation 39 days after synthesis before photoreduction stops. From 40 to 60 minutes of irradiation, the slight 0.37% increase in Ce(IV) absorbance at 290 nm indicates that the PAA-CeO_2 nanoparticles have begun to agglomerate.

Figure 10 shows UV-Vis absorption spectra of the PAA-La-CeO_2 sample taken every 10 minutes during UV irradiation 26 days after synthesis. During the first 30 minutes of irradiation, there is a 51% decrease in Ce(III) absorption at 290 nm which is accompanied by a significant blueshift of the absorption onset of the PAA-La-CeO_2 sample. Thus, during the first 30 minutes of irradiation, Ce(IV) centers within the PAA-La-CeO_2 sample are being reduced to Ce(III) centers. From 30 to 60 minutes of irradiation, there is a 7.6% increase in Ce(IV) absorption at 290 nm that can likely be attributed to the agglomeration of the nanoparticles.

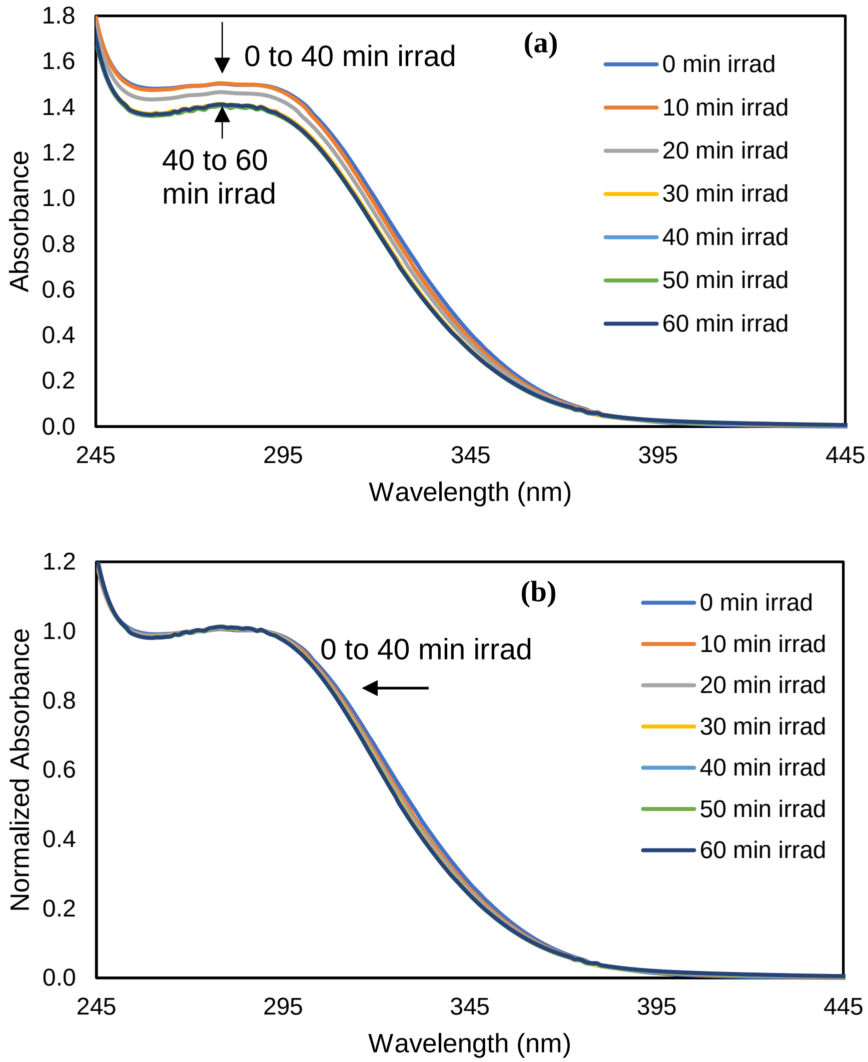

Figure 9. UV-Vis absorption spectra of the PAA-CeO_2 sample taken every 10 minutes during UV irradiaton 39 days after synthesis. (b) All UV-Vis absorption spectra in (a) normalized at 290 nm.

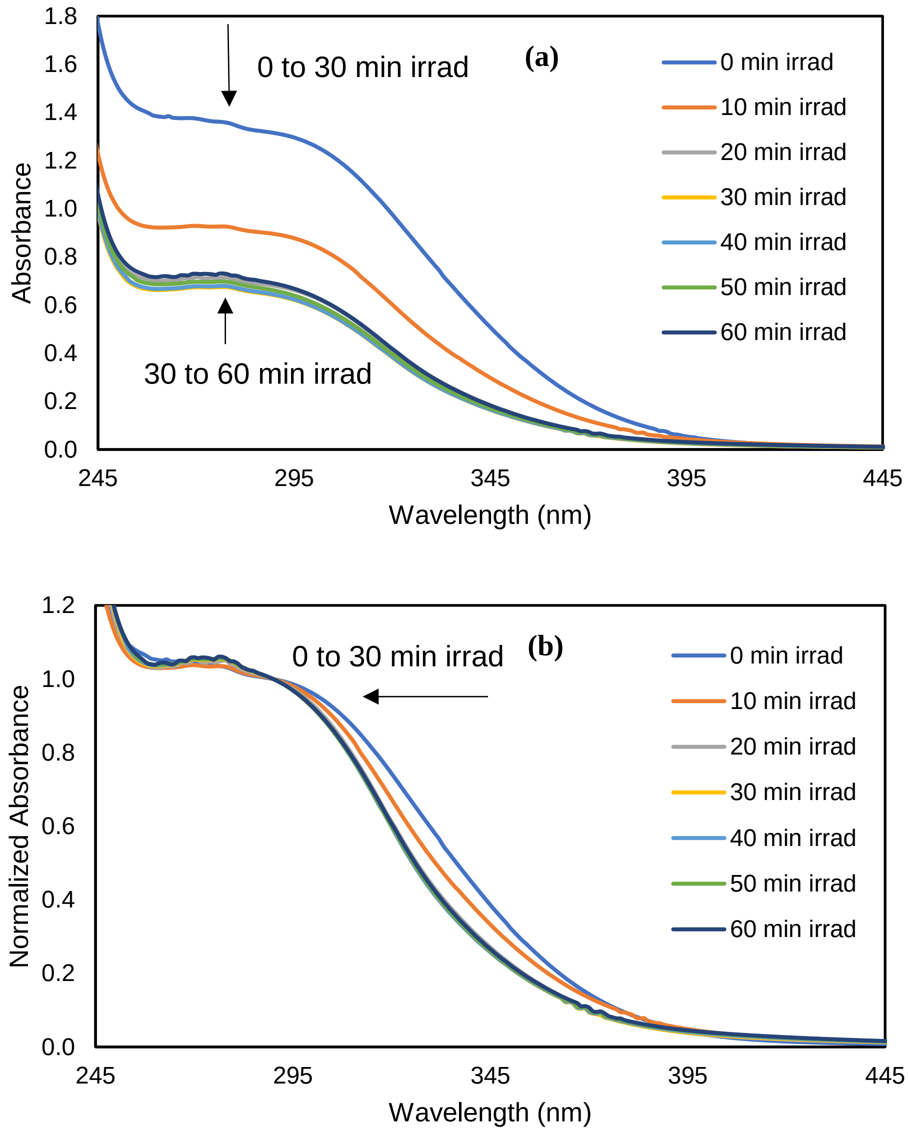

Figure 10. UV-Vis absorption spectra of the PAA-La-CeO_2 sample taken every 10 minutes during UV irradiation 26 days after synthesis. (b) All UV-Vis absorption spectra in (a) normalized at 290 nm.

UV-Vis absorption spectra of the PAA-La-CeO_2 sample taken every 10 minutes during UV irradiation 39 days after synthesis are shown in Figure 11. During the first 30 minutes of UV irradiation, there is a 61% decrease in Ce(IV) absorption at 290 nm accompanied by a prominent blueshift in the absorption onset of the PAA-La-CeO_2 sample. From 30 to 60 minutes of UV irradiation, there is a 10% increase in Ce(IV) absorbance at 290 nm. This indicates that during the first 30 minutes of UV irradiation, Ce(IV) centers within the PAA-La-CeO_2 sample are being reduced to Ce(III) before the nanoparticles begin to agglomerate in solution.

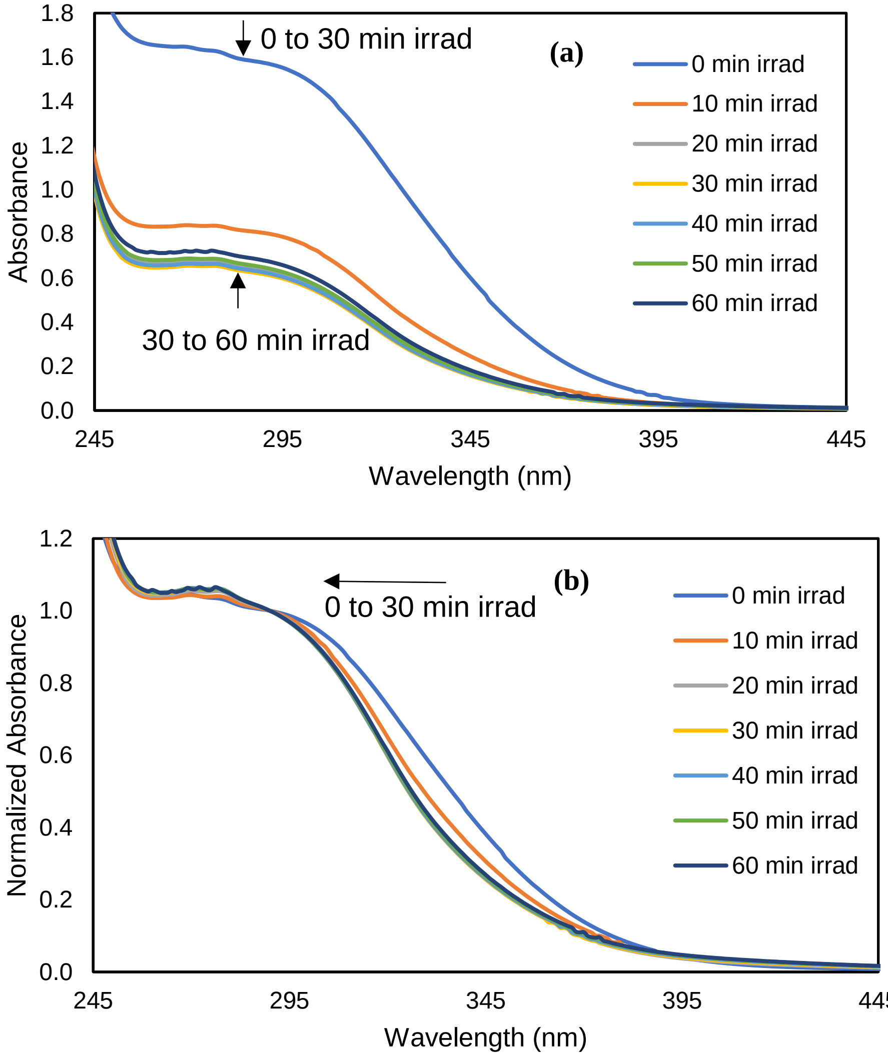

Figure 11. UV-Vis absorption spectra of the PAA-La-CeO_2 sample taken every 10 minutes during UV irradiation 39 days after synthesis. (b) All UV-Vis absorption spectra in (a) normalized at 290 nm.

The results of both sets of irradiation experiments performed 26 days and 39 days after the synthesis of the nanoceria samples show that the doped PAA-La-CeO_2 sample can be photoreduced to a greater extent than the pure PAA-CeO_2 sample. This could possibly be explained by the PAA-La-CeO_2 nanoparticles possessing a smaller size than the PAA-CeO_2 nanoparticles. Smaller ceria nanoparticles are expected to be more photoreducible than larger nanoparticles due to their increased surface-to-volume ratio, as photogenerated Ce(III) centers are expected to occupy surface sites of the nanoceria in pH 10 conditions (Pettinger, 2019). Therefore, a greater surface-to-volume ratio would allow for a greater percentage of the Ce(IV) present in the nanoceria to occupy the surface as photogenerated Ce(III) centers. Taniguchi et al. report that upon synthesis of Gd(III)-doped nanoceria, a decrease in crystallite size from 5.2 nm to 3.3 nm is seen when compared with pure nanoceria synthesized under the same experimental conditions (2008). This decrease in size is thought to be the result of Ce-O-Gd bonds suppressing the growth of the nanocrystals (Taniguchi et al., 2008). A similar decrease in size has also been seen in other syntheses of Gd-doped nanoceria via a coprecipitation method similar to the one performed in the synthesis of the PAA-La-CeO_2 sample (Godinho et al., 2006; Dikmen et al., 2002). Thus, although the same experimental conditions were used during the synthesis of the PAA-CeO_2 and the PAA-La-CeO_2 samples, further characterization via microscopic techniques such as transmission electron microscopy is needed to draw definite conclusions about particle size.

The increased photoreducibility of the PAA-La-CeO_2 sample is also consistent with the presence of increased oxygen vacancies within the lattice. Excitation by UV irradiation results in the formation of an electron-hole pair in the nanoceria. The electron localizes on Ce(IV) ions in the nanoceria, resulting in photogenerated Ce(III) centers. In pH 10 conditions, these Ce(III) centers migrate to the nanoceria surface, resulting in the formation of a Ce(III) surface layer. The photogenerated hole is scavenged by an adsorbed water molecule or polyacrylic acid capping ligand. Once the nanoceria surface is completely occupied by Ce(III) centers, photoreduction of the nanoceria is thought to cease, as photogenerated Ce(III) can no longer migrate to surface sites and can recombine with photogenerated holes in the nanoparticle. Oxygen vacancies are able to bind small polarons such as Ce(III) centers in nanoceria (Sun et al., 2017). Therefore, an increase in bulk oxygen vacancy concentration introduced into the nanoceria upon the incorporation of lanthanum into the lattice may be able to stabilize Ce(III) centers in the bulk of the nanoparticle, preventing the recombination of these centers with photogenerated holes. This would serve to increase the extent of photoreduction of the PAA-La-CeO_2 sample compared to the PAA-CeO_2 sample.

The increase in Ce(IV) absorbance at 290 nm seen after photoreduction of the PAA-CeO_2 sample 26 and 39 days after synthesis was found to be 0.95% and 0.37%, respectively. For the PAA-La-CeO_2 sample, the increase in Ce(IV) absorbance at 290 nm seen after photoreduction 26 and 39 days after synthesis was found to be much greater at 7.6% and 10%, respectively. This suggests that the PAA-La-CeO_2 nanoparticles agglomerate to a greater extent than the PAA-CeO_2 nanoparticles upon further UV irradiation after photoreduction. This is likely a result of the increased photoreducibility of the PAA-La-CeO_2 sample compared to the PAA-CeO_2 sample. As more photogenerated Ce(III) centers are produced in the PAA-La-CeO_2 sample, more photogenerated holes must be scavenged by the polyacrylic acid capping ligands. Therefore, degradation of polyacrylic acid is more pronounced for the PAA-La-CeO_2 sample during photoreduction, resulting in an increased agglomeration of the PAA-La-CeO_2 nanoparticles compared to the PAA-CeO_2 nanoparticles.

Monitoring the photogeneration of Ce(III) centers via fluorescence spectroscopy

Additional UV irradiation experiments were performed on the PAA-CeO_2 and PAA-La-CeO_2 samples to investigate whether changes in UV-Vis absorption spectra upon photoreduction of the nanoceria are correlated with changes in fluorescence emission spectra. To do this, UV-Vis absorption spectra, fluorescence emission spectra, and fluorescence excitation spectra were taken of the PAA-CeO_2 and PAA-La-CeO_2 samples immediately after each 10-minute irradiation interval with UV light from Hg lamps. In order to minimize reabsorption of emission by the nanoceria, the PAA-CeO_2 and PAA-La-CeO_2 samples were diluted so that their absorbances at 290 nm were 0.111 and 0.155, respectively.

Figure 12 displays UV-Vis absorption spectra of the PAA-CeO_2 sample taken every 10 minutes during UV irradiation. After the first fluorescence measurements taken of the PAA-CeO_2 sample prior to UV irradiation, the UV-Vis absorption of the PAA-CeO_2 sample was remeasured. Over the course of the fluorescence measurements taken prior to irradiation, the Ce(IV) absorption of the PAA-CeO_2 sample was found to increase by 8.1% at 290 nm. The reason for this slight increase in absorbance at 290 nm after fluorescence measurements prior to irradiation is unclear. During the first 10 minutes of irradiation, there is a 4.1% decrease in Ce(IV) absorption at 290 nm in the PAA-CeO_2 sample. This is accompanied by a slight blueshift in the absorption onset of the PAA-CeO_2, suggesting that Ce(III) centers are forming in the nanoceria during this time. Throughout the rest of the irradiation time, there is a 2.5% increase in Ce(IV) absorption at 290 nm likely due to agglomeration of the nanoparticles upon further irradiation.

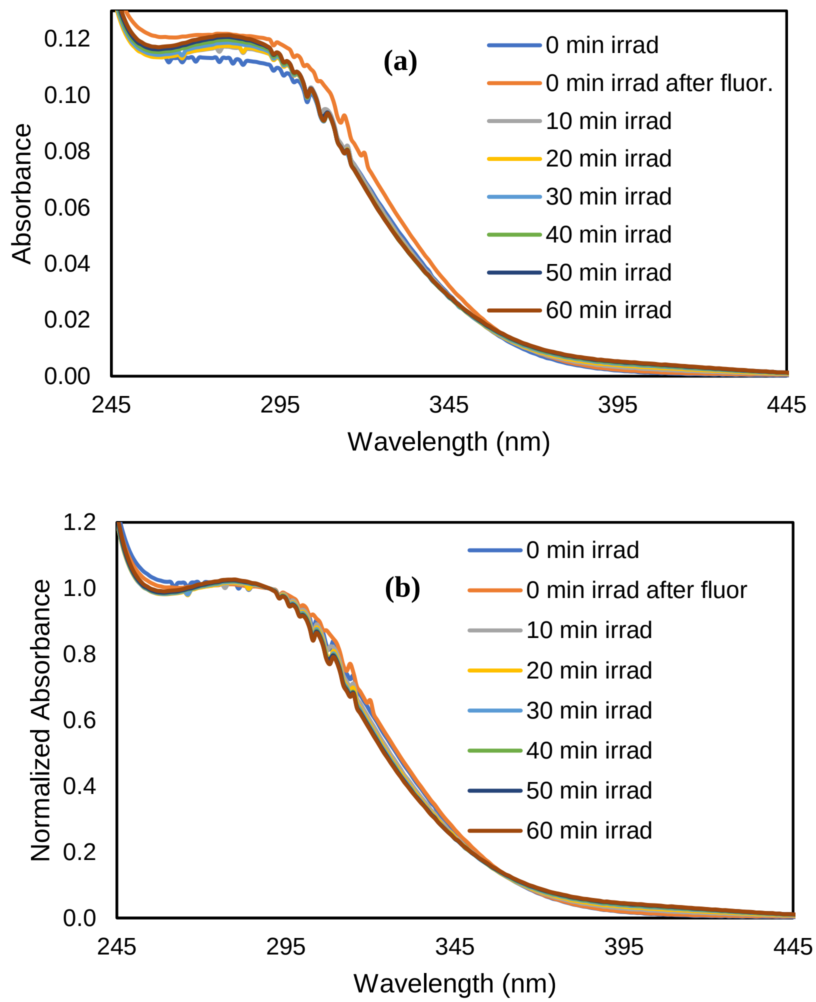

Figure 12. (a) UV-Vis absorption spectra of the PAA-CeO_2 sample taken every 10 minutes during UV irradiation. (b) UV-Vis absorption spectra in (a) normalized at 290 nm.

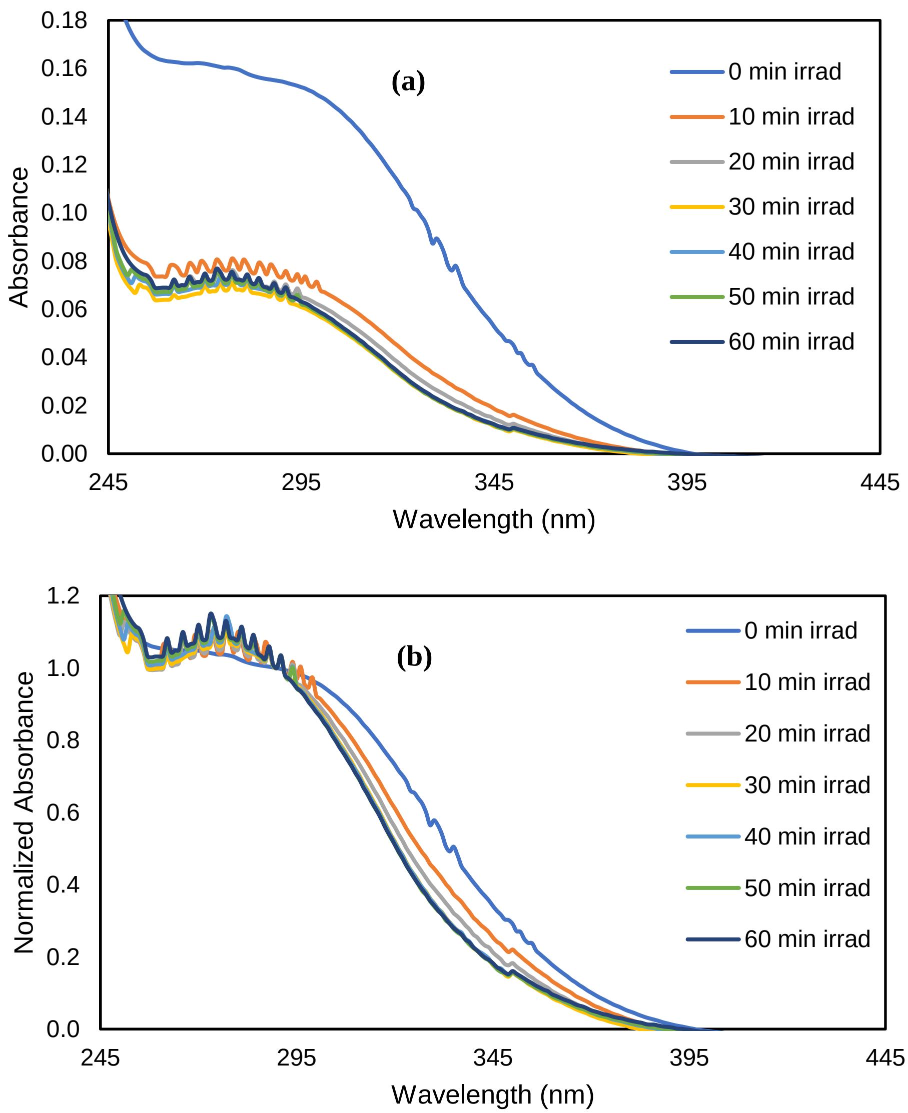

Figure 13. (a) UV-Vis absorption spectra of the PAA-La-CeO_2 sample taken every 10 minutes during UV irradiation. (b) UV-Vis absorption spectra in (a) normalized at 290 nm.

UV-Vis absorption spectra of the PAA-La-CeO_2 sample taken every 10 minutes during UV irradiation are shown in Figure 13. During the first 30 minutes of irradiation, there is a significant 59% decrease in Ce(IV) absorption at 290 nm in the PAA-La-CeO_2 sample. This is accompanied by a blueshift in the absorption onset of the PAA-La-CeO_2 sample. This suggests that during the first 30 minutes of irradiation, Ce(III) centers are being formed in the PAA-La-

CeO_2 sample. The 59% photoreduction seen in the PAA-La-CeO_2 sample during these UV irradiation experiments using fluorescence spectroscopy agrees well with the 51% and 61% photoreduction seen for more concentrated PAA-La-CeO_2 samples in the previously discussed UV irradiation experiments. From 30 to 60 minutes of irradiation, there is a 4.5% increase in Ce(IV) absorption at 290 nm which can be attributed to the agglomeration of the PAA-La-CeO_2 nanoparticles upon further UV irradiation.

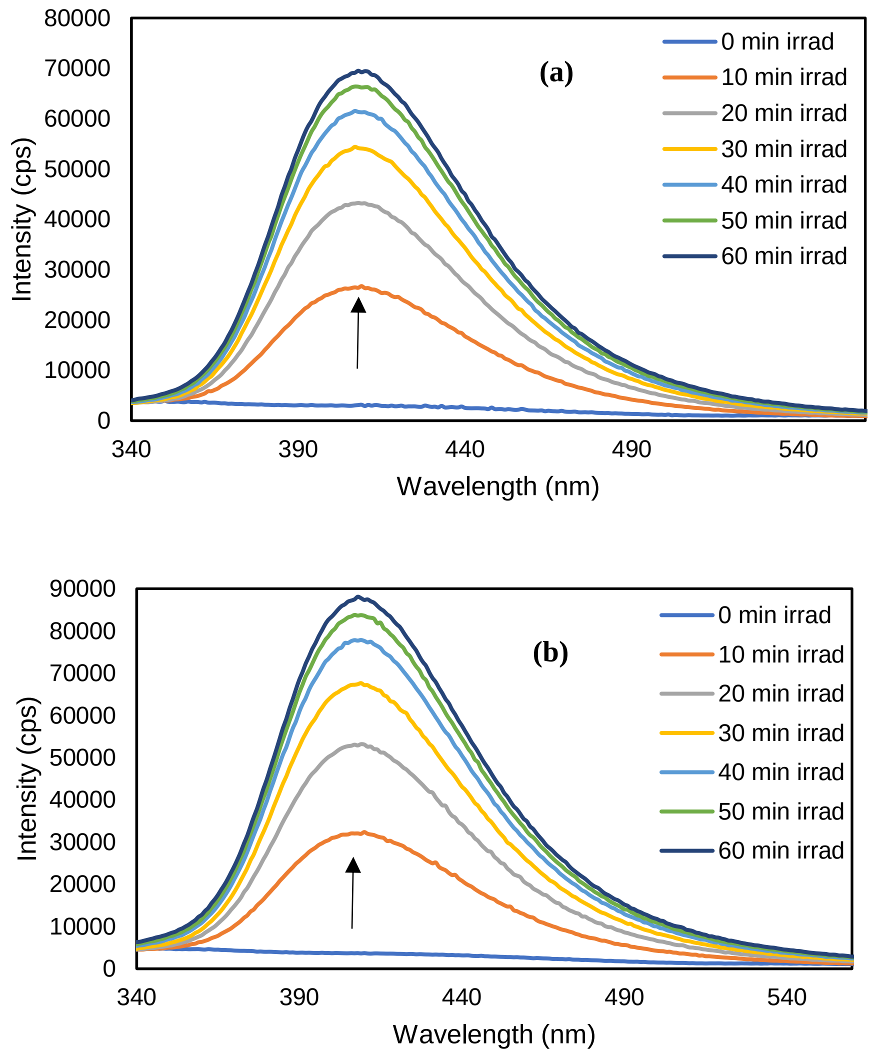

Figure 14. Fluorescence emission spectra of the (a) PAA-CeO_2 and (b) PAA-La-CeO_2 samples taken every 10 minutes during UV irradiation (λ_{ex} = 290 nm).

Figure 14 shows fluorescence emission spectra of the PAA-CeO_2 and PAA-La-CeO_2 samples taken every 10 minutes during UV irradiation with an excitation wavelength of 290 nm. Upon irradiation, there is the development of a strong emission peak at 410 nm in both samples which has been observed in previous work with photoreduced PAA-capped nanoceria in pH 10 conditions (Pettinger, 2019). The increase in emission at 410 nm is greatest in the first 10 minutes of irradiation. During subsequent 10-minute irradiation intervals, the increase in emission at 410 nm becomes less pronounced. To further investigate the origin of this emission at 410 nm, excitation spectra of the PAA-CeO_2 and PAA-La-CeO_2 samples were also taken every 10 minutes during UV irradiation with an emission wavelength of 410 nm, shown below in Figure 15. The excitation spectra show a broad double-peak with a maximum at 300 nm whose intensity increases with increasing irradiation time. In addition, there is a weaker peak at 360 nm that can be attributed to Raman scattering from the water solvent. Masalov et al. report that at 300 K, nanoceria that has been reduced in a hydrogen atmosphere displays emission centered at 390 nm from Ce(III) centers generated within the lattice (2014). An excitation spectrum of these H_2-reduced ceria nanocrystals taken at T = 10 K with an emission wavelength of 390 nm display a double peak that straddles 300 nm, similar to the double peak seen in the excitation spectra of the PAA-CeO_2 and PAA-La-CeO_2 samples (Masalov et al., 2014). In addition, Klochkov et al. report an increase in emission at approximately 425 nm after irradiating citrate-capped nanoceria with UV light (2018). Thus, the increase in emission at 410 nm upon UV irradiation of the PAA-CeO_2 and PAA-La-CeO_2 samples is likely due to the photoreduction of Ce(IV) centers within the nanoparticles to Ce(III).

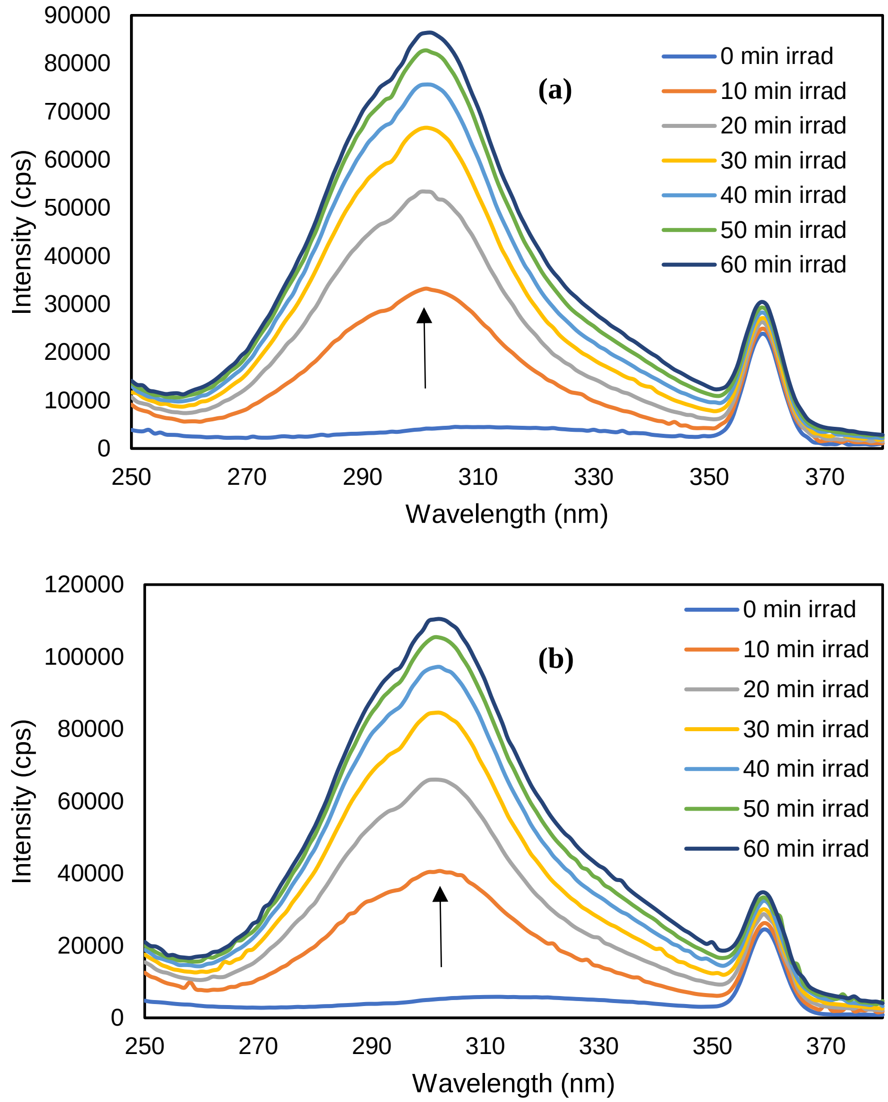

Figure 15. Fluorescence excitation spectra of the (a) PAA-CeO_2 and (b) PAA-La-CeO_2 samples taken every 10 minutes during UV irradiation (λ_{em} = 410 nm).

A graph of emission intensity at 410 nm vs. UV irradiation time for the PAA-CeO_2 (blue data series) and PAA-La-CeO_2 samples (orange data series) is displayed in Figure 16. Emission intensity at 410 nm rapidly increases before beginning to plateau for both samples; however, the emission intensity at 410 nm appears to increase more rapidly for the PAA-La-CeO_2 sample. Since the absorbance of the PAA-La-CeO_2 sample at 290 nm immediately before UV irradiation was greater than the initial absorbance of the PAA-CeO_2 sample immediately before UV irradiation (0.155 vs. 0.120), the number of excited states formed upon excitation with 290 nm light is expected to be greater in the PAA-La-CeO_2 sample than in the PAA-CeO_2 sample. This would result in a greater increase in emission at 410 nm upon UV irradiation of the PAA-La-CeO_2 sample that may be simply be a reflection of more Ce(IV) centers excited upon UV irradiation. The number of excited states formed in the PAA-CeO_2 and PAA-La-CeO_2 samples after excitation with 290 nm light scales with

$$1 - 10^{-A}$$

where A is the absorbance of the samples at 290 nm (Kohler, 2017). Using initial absorbance values of 0.155 and 0.120 for the PAA-La-CeO_2 and PAA-CeO_2 samples, respectively, the ratio of excited states formed in the PAA-La-CeO_2 sample to the excited states formed in the PAA-CeO_2 sample was calculated to be 1.237. Multiplying the emission intensity of the PAA-CeO_2 sample at 410 nm by 1.237 yields the gray data series in Figure 16 which is corrected for the difference in the number of excited states formed between the two samples. This new corrected plot of emission intensity at 410 nm vs. UV irradiation time for the PAA-CeO_2 sample matches the corresponding plot for the PAA-La-CeO_2 sample almost perfectly for the first 30 minutes of UV irradiation and very well for the last 30 minutes of UV irradiation. These results suggest that Ce(III) centers are forming in the PAA-CeO_2 and PAA-La-CeO_2 samples to very similar extents upon UV irradiation. However, the UV-Vis absorption spectra of the samples taken every 10 minutes during UV irradiation show that the decrease in Ce(IV) absorbance of the PAA-La-CeO_2 sample is significantly greater than the decrease in Ce(IV) absorbance of the PAA-CeO_2 sample upon irradiation (59% vs. 4%). Thus, results from UV-Vis absorption measurements suggest that the PAA-La-CeO_2 sample is more photoreducible than the PAA-CeO_2 sample, while results from fluorescence emission measurements suggest that the PAA-La-CeO_2 and PAA-CeO_2 samples are photoreduced to the same extent upon UV irradiation.

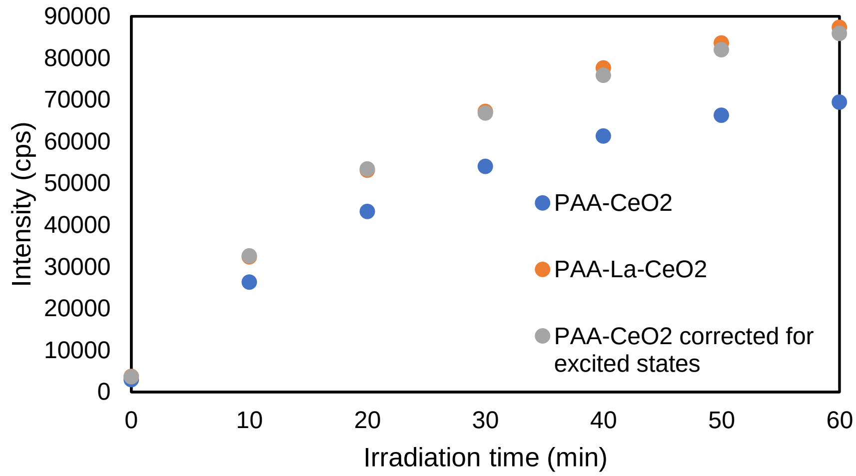

Figure 16. Fluorescence emission intensity at 410 nm as a function of UV irradiation time for the PAA-La-CeO_2 sample (orange data series), the PAA-CeO_2 sample (blue data series), and the PAA-CeO_2 sample corrected for the difference in the number of excited states between the PAA-CeO_2 and PAA-La-CeO_2 samples (gray data series).

This discrepancy could be explained by the fact that Ce(III) emission at 410 nm may be exclusively attributed to surface Ce(III) centers formed in the PAA-CeO_2 and PAA-La-CeO_2 samples upon irradiation. As proposed earlier, the increased photoreducibility of the PAA-La-CeO_2 sample could be explained by an increased bulk oxygen vacancy concentration due to the incorporation of the trivalent lanthanum dopant into the nanoceria lattice. Since oxygen vacancies are able to stabilize small polarons such as Ce(III) centers in nanoceria, photoreduction of the PAA-La-CeO_2 sample likely results in the formation of a greater concentration of bulk Ce(III) centers in addition to surface Ce(III) centers. The excitation of Ce(III) centers during fluorescence measurements promotes an electron in the Ce 4f band to the Ce 5d band. If the excited Ce(III) centers are stabilized by nearby positively-charged oxygen vacancies, then this could result in electron transfer between the excited Ce(III) center and the neighboring oxygen vacancy, which would subsequently relax nonradiatively. Quenching of fluorescence emission of trivalent rare earth ions due to electron transfer to oxygen vacancies has been reported in the literature. Kumar et al. report that in Eu(III)-doped nanoceria with Eu(III) concentrations above 15 mol %, a quenching of Eu(III) emission is observed due to an increase in nonradiative relaxation through oxygen vacancies (2009). Similar mechanisms of luminescence quenching have been proposed for Ce(III) ions in both ceria and other host lattices. First-principles calculations by Linderälv et al. suggest that the lowest energy pathway for thermal quenching of Ce(III) luminescence in Ce(III)-doped yttrium aluminum garnet ($Y_{3-x}Ce_xAl_5O_{12}$) is through charge transfer to oxygen vacancies (2021). Furthermore, Thajudheen et al. have reported that above a certain concentration, intrinsic oxygen vacancies in ceria quench its cathodoluminescence through strong associations of Ce(III) polarons with oxygen vacancies (2020). Oxygen vacancies are not thought to be present on the surface of nanoceria due to adsorption from water (Gritschneder and Reichling, 2007; Matolín et al., 2012); therefore, nonradiative relaxation pathways through charge transfer to neighboring oxygen vacancies are likely not available to photogenerated surface Ce(III) centers. Thus, the similar evolution in Ce(III) emission at 410 nm upon UV irradiation of the PAA-CeO_2 and PAA-La-CeO_2 samples may simply be a reflection of similar concentrations of surface Ce(III) centers being formed upon UV irradiation in the two samples. The increased photoreducibility of the PAA-La-CeO_2 would therefore not be apparent in the evolution of photogenerated Ce(III) emission over time, as it is likely the result of the increased formation of bulk Ce(III) centers which are able to relax nonradiatively through charge-transfer interactions with neighboring oxygen vacancies. If photogenerated Ce(III) emission at 410 nm can in fact be exclusively attributed to surface Ce(III) centers, then the excellent agreement in evolution of photogenerated Ce(III) emission at 410 nm throughout UV irradiation between the PAA-CeO_2 and PAA-La-CeO_2 samples provides evidence that the lanthanum-doped and pure ceria nanoparticles have similar sizes. This is because ceria nanoparticles with similar surface-to-volume ratios will form similar amounts of photogenerated Ce(III) centers on the surface throughout irradiation. This in turn would support the idea that the increased photoreducibility of the PAA-La-CeO_2 sample is due to an increase in bulk oxygen vacancy concentration upon the incorporation of lanthanum. However, additional characterization of the two samples is needed to confirm that the sizes of the PAA-La-CeO_2 and PAA-CeO_2 nanoparticles are similar.

There is a second discrepancy between the changes in Ce(IV) absorbance in the UV-Vis absorption spectra of the PAA-CeO_2 and PAA-La-CeO_2 samples and the changes in photogenerated Ce(III) emission at 410 nm upon UV irradiation that must be addressed. The decrease in Ce(IV) absorbance at 290 nm in the UV-Vis absorption spectra of the PAA-CeO_2 sample suggest that Ce(IV) centers are being photoreduced to Ce(III) only during the first 10 minutes of UV irradiation. Similarly, the decrease in Ce(IV) absorbance at 290 nm in the UV-Vis absorption spectra of the PAA-La-CeO_2 suggests that photoreduction occurs only during the first 30 minutes of UV irradiation for this sample. However, photogenerated Ce(III) emission at 410 nm is observed to increase throughout the entire 60-minute irradiation interval for both the PAA-CeO_2 and PAA-La-CeO_2 samples. One possible explanation for this discrepancy is that decreases in Ce(IV) absorbance at 290 nm due to the photogeneration of Ce(III) centers in the PAA-CeO_2 and PAA-La-CeO_2 samples after 10 and 30 minutes of UV irradiation, respectively, are offset by increases in Ce(IV) absorbance at 290 nm due to agglomeration of the nanoparticles upon further UV irradiation. The magnitude of the changes in Ce(IV) absorbance of the dilute

PAA-CeO_2 and PAA-La-CeO_2 samples at 290 nm seen after 10 minutes and 30 minutes of UV irradiation, respectively, are on the order of 0.005. Such small changes may be the sum of a small decrease in Ce(IV) absorbance at 290 nm due to photoreduction of the nanoceria and a larger increase in Ce(IV) absorbance at 290 nm due to agglomeration of the nanoceria, making it difficult to determine when photoreduction truly ceases in these samples.

Better conclusions about correlations between decreases in Ce(IV) absorbance at 290 nm and increases in photogenerated Ce(III) emission at 410 nm upon UV irradiation of the PAA-CeO_2 and PAA-La-CeO_2 samples can be drawn by repeating these experiments in order to confirm the reproducibility of the results. Repeating these experiments using more concentrated PAA-CeO_2 and PAA-La-CeO_2 samples with higher absorbances could also improve results by making changes in the UV-Vis absorption spectra of the samples upon UV irradiation more pronounced.

CONCLUSION

To observe the effect of increased oxygen vacancy concentration on the photochemistry of aqueous nanoceria, 25 mol % lanthanum-doped polyacrylic acid nanoceria was synthesized via a coprecipitation method. The incorporation of lanthanum was found to result in a decreased bandgap in the PAA-La-CeO_2 sample relative to the PAA-CeO_2 sample. Characterization via Raman spectroscopy could neither confirm nor rule out an increased oxygen vacancy concentration in the PAA-La-CeO_2 sample. The PAA-La-CeO_2 sample exhibited increased photoreducibility upon UV irradiation compared to the PAA-CeO_2 sample; however, further characterization is needed to determine whether this increased photoreducibility is due to a decrease in size of the nanoceria upon lanthanum incorporation or an increase in oxygen vacancy concentration that stabilizes the photogeneration of bulk Ce(III) centers in addition to surface Ce(III) centers. Lastly, excellent agreement in the evolution of photogenerated Ce(III) emission over time despite the increased photoreducibility of the PAA-La-CeO_2 suggests that Ce(III) emission at 410 nm could be exclusively due to photogenerated surface Ce(III) centers.

These results show that the incorporation of lanthanum significantly alters the photochemistry of aqueous nanoceria. These effects are likely due to the presence of bulk oxygen vacancies formed to compensate negative charge introduced into the nanoparticle through the incorporation of the trivalent dopant into the lattice. Thus, tuning the lanthanum concentration in aqueous nanoceria likely allows its photoreduction behavior upon UV irradiation to be manipulated. Increased control over the photochemistry of aqueous nanoceria through the incorporation of lanthanum(III) paves the way for the design of novel aqueous nanoceria photocatalysts. Possible future work includes varying the lanthanum content in aqueous polyacrylic acid-capped nanoceria more finely to gain a clearer picture of its effect on the photoreducibility of the nanoparticles. These studies can also be extended to aqueous nanoceria modified with other rare earth ions, such as europium(III) or gadolinium(III), to determine if effects on photoreducibility are dependent on the identity of the dopant ion or strictly a result of their 3+ charge.

REFERENCES

Asati, A.; Santra, S.; Kaittanis, C.; Nath, S.; Perez, J. M. Oxidase-Like Activity of Polymer-Coated Cerium Oxide Nanoparticles. *Angew. Chem., Int. Ed.* **2009**, *48*, 2308-2312, DOI: 10.1002/anie.200805279.

Bouchaud, B.; Balmain, J.; Bonnet, G.; Pedraza, F. pH-distribution of cerium species in aqueous systems. *J. Rare Earths* **2012**, *30*, 559-562, DOI: 10.1016/S1002-0721(12)60091-X.

Chahal, S.; Singh, S.; Kumar, A.; Kumar, P. Oxygen-deficient lanthanum doped cerium oxide nanoparticles for potential applications in spintronics and photocatalysis. *Vacuum* **2020**, *177*, 1-7, DOI: 10.1016/j.vacuum.2020.109395.

Chen, H.; Chang, H. Homogeneous precipitation of cerium dioxide nanoparticles in alcohol/water mixed solvents. *Colloids Surf., A* **2004**, *242*, 61-69, DOI: 10.1016/j.colsurfa.2004.04.056.

Damatov, D.; Laga, S. M.; Mader, E. A.; Peng, J.; Agarwal, R. G.; Mayer, J. M. Redox Reactivity of Colloidal Nanoceria and Use of Optical Spectra as an In Situ Monitor of Ce Oxidation States. *Inorg. Chem.* **2018**, *57*, 14401-14408, DOI: 10.1021/acs.inorgchem.8b02598.

Dikmen, S.; Shuk, P.; Greenblatt, M.; Gocmez, H. Hydrothermal synthesis and properties of $Ce_{1-x}Gd_xO_{2-\delta}$ solid solutions. *Solid State Sci.* **2002**, *4*, 585-590, DOI: 10.1016/S1293-2558(02)01301-8.

Dorenbos, P., The Electronic Structure of Lanthanide Doped Compounds with 3d, 4d, 5d, or 6d Conduction Band States. *J. Lumin.* **2014**, *151*, 224-228, DOI: 10.1016/j.jlumin.2014.02.019.

Godinho, M. J.; Gonçalves, R. F.; Santos, L. P. S.; Varela, J. A.; Longo, E.; Leite, E. R. Room temperature co-precipitation of nanocrystalline CeO_2 and $Ce_{0.8}Gd_{0.2}O_{1.9-\delta}$ powder. *Mater. Lett.* **2006**, *61*, 1904-1907, DOI: 10.1016/j.matlet.2006.07.152.

Gritschneder, S.; Reichling, M., Structural Elements of CeO2(111) Surfaces. *Nanotechnology* **2007**, *18*, 1-6, DOI: 10.1088/0957-4484/18/4/044024.

Keating, P. R. L.; Scanlon, D. O.; Watson, G. W. The nature of oxygen states of the surfaces of CeO_2 and La-doped CeO_2. *Chem. Phys. Lett.* **2014**, *608*, 239-243, DOI: 10.1016/j.cplett.2014.05.094.

Klochkov, V. K.; Malyukin, Yu. V.; Grygorova, G. V.; Sedyh, O. O.; Kavok, N. S.; Seminko, V. V.; Semynozhenko, V. P. Oxidation-reduction processes in CeO_{2-x} nanocrystals under UV irradiation. *J. Photochem. Photobiol., A* **2018**, *364*, 282-287, DOI: 10.1016/j.jphotochem.2018.06.025.

Kohler, B. Excited States of Single-Stranded DNA Revealed by Femtosecond Transient Absorption Spectroscopy. In *Ultrafast Dynamics at the Nanoscale: Biomolecules and Supramolecular Assemblies;* Burghardt, I.; Haacke, S., Eds.; Pan Stanford Publishing: Singapore, 2017; 1-62.

Kumar, A.; Babu, S.; Karakoti, A. S.; Schulte, A.; Seal, S. Luminescence Properties of Europium-Doped Cerium Oxide Nanoparticles: Role of Vacancy and Oxidation States. *Langmuir* **2009**, *25*, 10998-11007, DOI: 10.1021/la901298q.

Linderälv, C.; Åberg, D.; Erhart, P. Luminescence Quenching via Deep Defect States: A Recombination Pathway via Oxygen Vacancies in Ce-Doped YAG. *Chem. Mater.* **2021**, *33*, 73-80, DOI: 10.1021/acs.chemmater.0c02449.

Marabelli, F.; Wachter, P. Covalent insulator CeO_2: Optical reflectivity measurements. *Phys. Rev. B.* **1987**, *36*, 1238-1243, DOI: 10.1103/PhysRevB.36.1238.

Masalov, A.; Viagin, O.; Maksimchuk, P.; Seminko, V.; Bespalova, I.; Aslanov, A.; Malyukin, Y.; Zorenko, Y. Formation of luminescent centers in CeO_2 nanocrystals. *J. Lumin.* **2014**, *145*, 61-64, DOI: 10.1016/j.jlumin.2013.07.020.

Matolín, V.; Matolínová, I.; Dvořák, F.; Johánek, V.; Mysliveček, J.; Prince, K. C.; Skála, T.; Stetsovych, O.; Tsud, N.; Václavů, M.; Šmíd, B., Water Interaction with CeO2(1 1 1)/Cu(1 1 1) Model Catalyst Surface. *Catal. Today* **2012**, *181*, 124-132, DOI: 10.1016/j.cattod.2011.05.032.

McBride, J. R.; Hass, K. C., Poindexter, B. D., Weber, W. H. Raman and x-ray studies of $Ce_{1-x}RE_xO_{2-y}$, where RE=La, Pr, Nd, Eu, Gd, and Tb. *J. Appl. Phys.* **1994**, *76*, 2435-2441, DOI: 10.1063/1.357593.

Montini, T.; Melchionna, M.; Monai, M.; Fornasiero, P. Fundamentals and Catalytic Applications of CeO_2-Based Materials. *Chem. Rev.* **2016**, *116*, 5987-6041, DOI: 10.1021/acs.chemrev.5b00603.

Pettinger, N. W. The Charge-Carrier Dynamics and Photochemistry of CeO_2 Nanoparticles. Ph.D. Dissertation, The Ohio State University, Columbus, OH, 2019.

Pettinger, N. W.; Empey, J. M.; Fröbel, S.; Kohler, B. Photoreductive dissolution of cerium oxide nanoparticles and their size-dependent absorption properties. *Phys. Chem. Chem. Phys.* **2020**, *22*, 5756-5764, DOI: 10.1039/c9cp06579b.

Sun, L.; Huang, X.; Wang, L.; Janotti, A. Disentangling the role of small polarons and oxygen vacancies in CeO_2. *Phys. Rev. B.* **2017**, *95*, 245101, DOI: 10.1103/PhysRevB.95.245101.

Taniguchi, T.; Watanabe, T.; Sakamoto, N.; Matsushita, N.; Yoshimura, M. Aqueous Route to Size-Controlled and Doped Organophilic Ceria Nanocrystals. *Cryst. Growth Des.* **2008**, *8*, 3725-3730, DOI: 10.1021/cg800363w.

Thajudheen, T.; Dixon, A. G.; Gardonio, S.; Arčon, I.; Valant, M. Oxygen Vacancy-Related Cathodoluminescence Quenching and Polarons in CeO_2. *J. Phys. Chem. C* **2020**, *124*, 19929-19936, DOI: 10.1021/acs.jpcc.0c04631.

Zhang, B.; Li, D.; Wang, X. Catalytic performance of La-Ce-O mixed oxide for combustion of methane. *Catal. Today* **2010**, *158*, 348-353, DOI: 10.1016/j.cattod.2010.04.019.